Retinal neurodegeneration may precede microvascular changes characteristic of diabetic retinopathy in diabetes mellitus

Elliott H. Sohn[a,1], Hille W. van Dijk[b,1], Chunhua Jiao[a], Pauline H. B. Kok[b], Woojin Jeong[a], Nazli Demirkaya[b], Allison Garmager[a], Ferdinand Wit[c], Murat Kucukevcilioglu[a], Mirjam E. J. van Velthoven[d], J. Hans DeVries[e], Robert F. Mullins[a], Markus H. Kuehn[a], Reinier Otto Schlingemann[b], Milan Sonka[f,g], Frank D. Verbraak[b,h], and Michael David Abràmoff[a,f,g,i,j,2]

[a]Stephen A. Wynn Institute for Vision Research, Department of Ophthalmology, University of Iowa, Iowa City, IA 52242; [b]Department of Ophthalmology, Academic Medical Center, University of Amsterdam, 1105 AZ Amsterdam, The Netherlands; [c]Department of Global Health, Academic Medical Center, University of Amsterdam, 1105 AZ Amsterdam, The Netherlands; [d]Oogziekenhuis Rotterdam, 3011 BH Rotterdam, The Netherlands; [e]Department of Endocrinology, Academic Medical Center, University of Amsterdam, 1105 AZ Amsterdam, The Netherlands; [f]Iowa Institute for Biomedical Imaging, University of Iowa, Iowa City, IA 52242; [g]Department of Electrical and Computer Engineering, University of Iowa, Iowa City, IA 52242; [h]Department of Biomedical Engineering and Physics, Academic Medical Center, University of Amsterdam, 1105 AZ Amsterdam, The Netherlands; [i]Iowa City VA Health Care System, Iowa City, IA 52246; and [j]Department of Biomedical Engineering, University of Iowa, Iowa City, IA 52242

Edited by Artur V. Cideciyan, University of Pennsylvania, Philadelphia, PA, and accepted by the Editorial Board March 23, 2016 (received for review December 17, 2015)

Diabetic retinopathy (DR) has long been recognized as a microvasculopathy, but retinal diabetic neuropathy (RDN), characterized by inner retinal neurodegeneration, also occurs in people with diabetes mellitus (DM). We report that in 45 people with DM and no to minimal DR there was significant, progressive loss of the nerve fiber layer (NFL) (0.25 μm/y) and the ganglion cell (GC)/inner plexiform layer (0.29 μm/y) on optical coherence tomography analysis (OCT) over a 4-y period, independent of glycated hemoglobin, age, and sex. The NFL was significantly thinner (17.3 μm) in the eyes of six donors with DM than in the eyes of six similarly aged control donors (30.4 μm), although retinal capillary density did not differ in the two groups. We confirmed significant, progressive inner retinal thinning in streptozotocin-induced "type 1" and *B6.BKS(D)-Lepr^{db}/J* "type 2" diabetic mouse models on OCT; immunohistochemistry in type 1 mice showed GC loss but no difference in pericyte density or acellular capillaries. The results suggest that RDN may precede the established clinical and morphometric vascular changes caused by DM and represent a paradigm shift in our understanding of ocular diabetic complications.

diabetes | retina | neurodegeneration | diabetic retinopathy | optical coherence tomography

Diabetic retinopathy (DR), the most common cause of irreversible blindness in working-age adults, results in central vision loss caused by microvascular damage to the inner lining of the back of the eye known as the retina (1). Diabetes mellitus (DM) is accompanied by retinal diabetic neuropathy (RDN), i.e., inner neuroretinal degeneration; this neuropathy is observed structurally, as neural apoptosis, ganglion cell (GC) loss, reactive gliosis, and thinning of the inner retina; and functionally, as deficits in the electroretinogram (ERG), dark adaptation, contrast sensitivity, color vision, and microperimetric and perimetric psychophysical testing (2–5). Because the neuroretina forms an extension of the brain embryologically, functional retinal changes may correlate with the cognitive decline in people with DM (6). Studies have shown that local functional loss on pattern ERG, which measures GC function, predicts local microvasculopathy and macular edema 1 y later (7). Pericyte loss is defined as the earliest detectable microvascular marker of DR in the retina (8), whereas microaneurysms on funduscopy or fundus photographs are defined as the first marker of clinically manifest DR (9). So-called "preclinical diabetic retinopathy" comprises additional vascular abnormalities such as acellular capillaries (10–14).

Although ample evidence suggests that retinal damage, including clinically detectable DR and macular edema, results from microvascular abnormalities, the relationship between RDN and microvascular damage is unclear. Most assume that RDN is a secondary effect of microvascular damage, but mounting evidence shows that neuroretinal alterations are present even in the absence of clinically detectable retinal vasculopathy, i.e., DR, both in donor eyes of people with DM and on retinal optical coherence tomography (OCT) image analysis (4, 14–18). However, these studies were unable to show the temporal relationship between

Significance

Diabetic retinopathy (DR), a primary cause of blindness, is characterized by microvascular abnormalities. Recent evidence suggests that retinal diabetic neuropathy (RDN) also occurs in people with diabetes, but little is known about the temporal relationship between DR and RDN. This longitudinal study in people with diabetes with no or minimal DR shows that RDN precedes signs of microvasculopathy and that RDN is progressive and independent of glycated hemoglobin, age, and sex. This finding was further confirmed in human donor eyes and in two experimental mouse models of diabetes. The results suggest that RDN is not ischemic in origin and represent a shift in our understanding of the pathophysiology of this complication of diabetes that potentially affects vision in all people with diabetes mellitus.

Author contributions: E.H.S., H.W.v.D., C.J., J.H.D., R.O.S., F.D.V., and M.D.A. designed research; E.H.S., H.W.v.D., C.J., P.H.B.K., W.J., N.D., A.G., F.W., M.K., M.E.J.v.V., J.H.D., R.F.M., M.H.K., R.O.S., F.D.V., and M.D.A. performed research; M.S. and M.D.A. contributed new reagents/analytic tools; E.H.S., C.J., F.W., F.D.V., and M.D.A. analyzed data; E.H.S., H.W.v.D., F.D.V., and M.D.A. wrote the paper; H.W.v.D., C.J., P.H.B.K., W.J., N.D., A.G., M.K., M.E.J.v.V., R.F.M., M.H.K., F.D.V., and M.D.A. managed data acquisition; and E.H.S., C.J., F.W., R.F.M., M.H.K., R.O.S., M.S., F.D.V., and M.D.A. provided administrative, technical, or material support.

Conflict of interest statement: M.D.A. has direct equity ownership of and receives income from IDx LLC, a company that has licensed inventions from the University of Iowa, on which the Iowa Reference Algorithms used in this study are based. M.D.A. and M.S. are inventors on patents assigned to the University of Iowa and licensed by IDx LLC.

This article is a PNAS Direct Submission. A.V.C. is a guest editor invited by the Editorial Board.

The Iowa Reference Algorithms used for automated analysis of the human and mouse OCT data are freely available to all researchers in the public domain at www.iibi.uiowa.edu/content/shared-software-download/. Underlying data are available from M.D.A. (michael-abramoff@uiowa.edu) on request.

[1]E.H.S. and H.W.v.D. contributed equally to this work.

[2]To whom correspondence should be addressed. Email: michael-abramoff@uiowa.edu.

This article contains supporting information online at www.pnas.org/lookup/suppl/doi:10.1073/pnas.1522014113/-/DCSupplemental.

RDN and vasculopathy (19, 20). The purpose of this study was to determine the time course of inner retinal neurodegeneration in relation to microvasculopathy in people with DM with no or minimal clinically detectable microvascular DR and to determine whether these findings are further supported by experimental murine models of DM.

Results

Longitudinal Human Study. Forty-five patients with type 1 DM (mean age 31 ± 10 y) were enrolled in this prospective, longitudinal study. At baseline, 21 patients had no DR, and 24 patients showed minimal DR. None of the patients had a central subfield retinal thickness over 250 μm, which is the cutoff for diabetic macular edema in the Diabetic Retinopathy Clinical Research Network studies for time-domain OCT (21). During follow-up, 18 patients demonstrated progression of DR. The mean glycated hemoglobin (HbA1c) at baseline was 8.2% (SD 1.2%). There were no statistically significant changes in mean HbA1c, blood pressure, or best corrected visual acuity (BCVA) during the four study visits. The median follow-up time was 73.0 mo (range, 37–79 mo; interquartile range, 57.5–80 mo). Six patients skipped intermediary visits, and 10 were lost to follow-up because of migration (Table S1).

The thickness of the inner retinal layers of the macula —the nerve fiber layer (NFL), GC layer (GCL), and inner plexiform layer (IPL)—decreased significantly over time, after adjustment for sex, age at inclusion, duration of DM before inclusion, HbA1c, presence of DR at inclusion, and progression of DR after inclusion (Fig. 1 and Table 1). Specifically, the amount of thinning for the NFL in the macula was 0.25 μm/y both parafoveally [95% confidence interval (CI), −0.40 to −0.11 μm/y, $P < 0.001$] and perifoveally (95% CI, −0.42 to −0.08 μm/y, $P = 0.004$). For the GCL+IPL the amount of thinning was 0.29 μm (95% CI, −0.49 to −0.08 μm, $P = 0.006$) parafoveally; there was no significant change in the perifoveal GCL+IPL (95% CI, −0.04 to 0.36 μm) (Fig. 2 and Fig. S1).

Subjects with longer duration of DM before inclusion started with thinner macular NFL and thinner GCL+IPL at inclusion (Table 1). This prestudy thinning as a result of DM was in close agreement with the NFL and GCL+IPL loss per year observed during the study period: Each year of DM duration before inclusion was associated with a 0.19- to 0.21-μm thinner macular NFL and with a 0.11- to 0.44-μm thinner macular GCL+IPL at inclusion. Neither the presence of any DR at inclusion, nor progression of DR after inclusion was associated with any change in the NFL or GCL+IPL, nor did age, blood pressure, or HbA1c level influence the thickness of the NFL or GCL-IPL. As expected, female sex was associated with significantly thinner parafoveal NFL and GCL at inclusion (22).

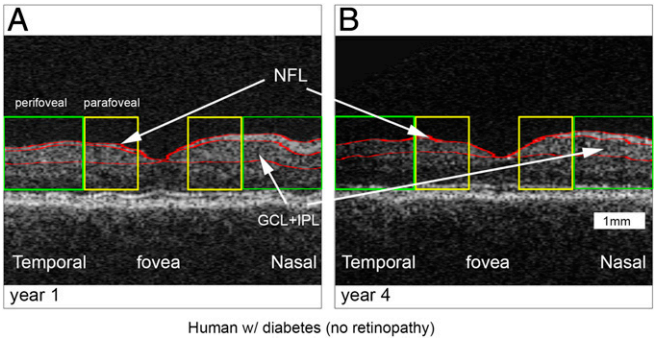

Fig. 1. Stratus OCT (horizontal B-scans through the fovea) automated analysis of the right eye of one of the subjects, a 42-y-old female without DR, at the baseline visit (*A*) and at the fourth-year visit (*B*) showing generalized loss of the NFL and GCL+IPL over this time period in the parafoveal (yellow outline) and perifoveal (green outline) regions (see Fig. S1*B*). The top red line is the ILM that represents the inner boundary of the retina separating the vitreous cavity and the NFL. The middle red line is the boundary between the NFL and the GCL. The bottom red line is the boundary between the IPL and INL. At year 4 (*B*), the loss of the NFL is so profound in this subject that it is hard to differentiate the top and middle red lines on the temporal (left) side of the fovea. (Scale bar, 1 mm; the width of the scan is 6 mm.)

Results from Donor Eyes. We included six eyes from deceased donors with DM and no or minimal DR and six eyes from similarly aged deceased donors without DM (Table S2). In the five eyes from DM donors with sufficient tissue quality, the NFL was significantly ($P = 0.03$) thinner (17.3 μm; 95% CI, 13.18–21.38 μm) than in five eyes from the control group (30.4 μm; 95% CI, 22.37–38.47 μm) (Fig. 3 and Fig. S2). GC density was not significantly different in the five eyes from the DM group (11.5 GC/1,000 μm; 95% CI, 6.49–16.56 GC/1,000 μm) and the five eyes from the control group (14.1 GC/1,000 μm; 95% CI, 13.28–15.01 GC/1,000 μm) ($P = 0.37$). No significant difference in retinal capillary density ($P = 0.13$) was seen among all eyes in the DM group (0.18; 95% CI, 0.15–0.18) and all eyes in the control group (0.17; 95% CI, 0.17–0.20) (Fig. S3).

Results from the Streptozotocin-Induced Type 1 DM Mouse Model. Mice in the streptozotocin (STZ)-treated group (a type 1 DM model) and C57BL/6J age-matched controls (Fig. S4) underwent OCT image analysis at 6 wk ($n = 21$ DM, $n = 15$ controls) and 20 wk ($n = 11$ DM, $n = 10$ controls) of DM duration (Fig. S5). We found that at 6 wk after DM induction the NFL+GCL was significantly thinner in the STZ group (8.97 μm; 95% CI, 8.00–9.59 μm) than in the control group (10.54 μm; 95% CI, 10.10–10.98 μm), an average difference of 1.57 μm (17.5%). This thinning in the STZ group as compared with controls progressed with time: At 20 wk of DM duration, the STZ group had an NFL+GCL thickness of 6.45 μm (95% CI, 5.89–7.02 μm), whereas controls had a thickness of 8.98 μm (95% CI, 8.24–9.72 μm), an average difference of 2.53 μm (39.2%) (Fig. 4*A*). In the control group, there was significant age-related thinning of the NFL+GCL of 0.084 μm/wk (95% CI, 0.073–0.095 μm/wk, $P = 0.001$), whereas in the STZ group DM causes significantly accelerated NFL+GCL thinning of 0.218 μm/wk (95% CI, 0.212–0.224 μm/wk, $P < 0.001$).

Immunohistochemistry of a subset of the mice used in the OCT imaging study at 6 wk after DM induction showed no reduction ($P = 0.560$) in GC density in STZ mice (45.7%; 95% CI, 43.6–47.8%, $n = 10$) compared with C57BL/6J age-matched controls (44.7%; 95% CI, 42.9–46.4%, $n = 9$). However, at 20 wk after DM induction we found significant ($P = 0.008$) loss of GC density in STZ mice (STZ mice: 45.8%; 95% CI, 44.2–47.4%, $n = 10$; controls: 50.2%; 95% CI, 48.2–52.2%, $n = 10$) (Fig. 4 *B*–*D*).

To compare microvasculopathy in the STZ group and controls, we examined capillaries and pericytes in the contralateral eyes of the mice used for the GC study. At 6 wk after DM induction, there was no difference between the STZ group and controls in the density of endothelial-supporting retinal pericytes (STZ group: 0.33; 95% CI, 0.31–0.35; controls: 0.33; 95% CI, 0.32–0.33, $P = 0.72$) or in the percentage of acellular capillaries in trypsin-digested retina (STZ group: 1.1%; 95% CI, 0.8–1.4%; controls: 0.9%; 95% CI, 0.7–1.1%, $P = 0.22$) (Fig. 5). Microvascular changes typically occur in these diabetic mice between 18 and 24 wk after DM induction (19), but even at 20 wk pericyte density was not statistically different in the NFL/GCL (STZ group: 0.74; 95% CI, 0.78–1.02; controls 0.90; 95% CI, 0.62–0.85; $P = 0.063$) (Fig. 5*C*) or in the inner (STZ group: 0.23, 95% CI, 0.20–0.27; controls: 0.27; 95% CI, 0.23–0.30; $P = 0.30$) and outer (STZ group: 0.43: 95% CI, 0.40–0.46; controls: 0.47; 95% CI, 0.41–0.51; $P = 0.18$) vascular plexus. We measured retinal microvessel density using *Griffonia simplicifolia* IB4 isolectin (GSL-IB4) at 20 wk and found no significant difference ($P = 0.11$) between the STZ group (0.0089; 95% CI, 0.0115–0.0091) and controls (0.0103; 95% CI, 0.0101–0.0077).

Table 1. Changes per year in the thickness of the parafoveal and perifoveal rings of the retinal NFL and GCL+IPL in patients with type 1 DM with no or minimal DR

Independent variable	Parafoveal NFL	Perifoveal NFL	Parafoveal GCL+IPL	Perifoveal GCL+IPL
Intercept	**15.05 μm, $P < 0.001$** (95% CI, 10.05–20.05 μm)	**38.72 μm, $P < 0.001$** (95% CI, 32.68–44.76 μm)	**104.18 μm, $P < 0.001$** (95% CI, 93.58–114.78 μm)	**71.21 μm, $P < 0.001$** (95% CI, 65.40–77.03μm)
Female sex	**−1.79 μm, $P = 0.008$** (95% CI, −3.10 to −0.48 μm)	−0.27 μm, $P = 0.739$ (95% CI, −1.84 to 1.31 μm)	**−4.22 μm, $P = 0.012$** (95% CI, −7.49 to −0.95 μm)	**0.11 μm, $P = 0.896$** (95% CI, −1.50 to 1.71 μm)
Age at inclusion, y	0.08 μm, $P = 0.135$ (95% CI, −0.02 to 0.15 μm)	−0.02 μm, $P = 0.612$ (95% CI, −0.13 to 0.08 μm)	0.04 μm, $P = 0.786$ (95% CI, −0.19 to 0.27μm)	−0.06 μm, $P = 0.374$ (95% CI, −0.15 to 0.06 μm)
Duration prior DM, y	**−0.19 μm, $P = 0.002$** (95% CI, −0.30 to −0.08 μm)	**−0.21 μm, $P = 0.005$** (95% CI, −0.34 to −0.06 μm)	**−0.44 μm, $P = 0.004$** (95% CI, -0.74 to −0.13)	−0.11 μm, $P = 0.120$ (95% CI, −0.27 to 0.04 μm)
Follow-up, y	**−0.25 μm, $P < 0.001$** (95% CI, −0.40 to −0.11 μm)	**−0.25 μm, $P = 0.004$** (95% CI, −0.42 to −0.08 μm)	**−0.29 μm, $P = 0.006$** (95% CI, −0.49 to −0.08 μm)	0.19 μm, $P = 0.021$ (95% CI, 0.04–0.36 μm)
Minimal DR at inclusion, present/absent	1.03 μm, $P = 0.203$ (95% CI, −0.55 to 2.60 μm)	−0.19 μm, $P = 0.838$ (95% CI, −2.09 to 1.69 μm)	1.71 μm, $P = 0.361$ (95% CI, −1.98 to 5.38 μm)	0.17 μm, $P = 0.864$ (95% CI, −1.73 to 2.05 μm)
DR grade	0.06 μm, $P = 0.815$ (95% CI, −0.48 to 0.61 μm)	0.06 μm, $P = 0.855$ (95% CI, −0.59 to 0.70 μm)	−0.63 μm, $P = 0.147$ (95% CI, −1.48 to 0.23 μm)	−0.32 μm, $P = 0.283$ (95% CI, −0.93 to 0.29 μm)
HbA1c, %	0.13 μm, $P = 0.432$ (95% CI, −0.19 to 0.46 μm)	−0.40 μm, $P = 0.048$ (95% CI, μm 0.80 to −0.00 μm)	0.06 μm, $P = 0.811$ (95% CI, −0.42 to 0.53μm)	0.17 μm, $P = 0.366$ (95% CI, −0.19 to 0.51 μm)

Shown are the change in thickness per year (in micrometers) per one unit change of each independent variable, the *P* value, and the 95% CI. Significant changes are shown in boldface type. Blood pressure and DR progression were not significantly associated.

Results from the *db/db* Type 2 DM Mouse Model. Although the attenuation of the GCL and the NFL in the STZ-induced type I DM mouse model was likely attributable to DM, we evaluated the possibility that STZ had a direct toxic effect on the inner retina (23) in the *db/db* mouse model of spontaneous DM, using in vivo OCT imaging analysis of the retina. The *db/db* group showed significant thinning of the NFL+GCL as compared with age-matched control mice at both age 10 wk [9.47 μm (95% CI, 8.75–10.18 μm) vs. 11.00 μm (95% CI, 10.34–11.66 μm), $P = 0.01$] and age 16 wk [8.08 μm (95% CI, 7.62–8.53 μm) vs. 10.11 μm (95% CI, 8.80–11.42 μm), $P = 0.02$] (Fig. 6). We also found a significantly accelerated thinning of the NFL+GCL of 0.104 μm/wk (95% CI, 0.086–0.123 μm/wk, $P < 0.001$) in the *db/db* group.

Discussion

The longitudinal results show that inner RDN may occur before signs of microvasculopathy or DR in people with DM, according to widely accepted definitions by Cogan (8) and Friedenwald (9), respectively. Additionally, the results in donor eyes from people with DM and no or minimal DR and in two different experimental mouse models of DM confirm that RDN may precede DR. RDN is progressive over the course of DM both in humans and mice and outstrips the neurodegeneration associated with normal aging. These key findings are supported by multiple parallel, but independent, assays for retinal neurodegeneration and vascular abnormalities: OCT imaging analysis, fundus imaging, and immunohistochemistry in diabetic humans and mouse models of DM.

Specifically, using OCT image analysis in a 4-y longitudinal study of people with DM with no or minimal DR on fundus examination, we found a significant, progressive loss in the NFL (0.25 μm/y) and GCL+IPL (0.29 μm/y) that was independent of HbA1C, DR, or progression of DR. This progressive neuroretinal degeneration was primarily related to DM duration, and not to HbA1C (Table 1). Using these same methods, we have previously shown that, in normal subjects in the same age range without DM, the NFL thins by 0.133 μm/y parafoveally, and the GCL+IPL thins by 0.149 μm/y parafoveally (Figs. 1 and 2 and Table 1) (14). These findings confirm earlier cross-sectional findings of neuroretinal degeneration in DM, independent of DR, by our group (4, 15, 16) and others (24) and show, for the first time to our knowledge, that this loss continues over the course of the disease. Postmortem study of the inner retina of human donors allowed us to confirm at the histologic level that the NFL is significantly thinner, without alterations in retinal capillary density, in persons who had DM with no to minimal DR compared with age-matched controls, Fig. 3.

We also evaluated two mouse models of DM to characterize the temporal sequence of the observed changes directly, through both OCT image analysis and immunohistochemistry at the microscopic level, analyses that are exceptionally difficult in humans. The STZ group had significant thinning of the NFL+GCL on OCT image analysis, as compared with the age-matched control group, at both 6 wk and 20 wk after DM induction, and this difference increased over time, with a loss of 1.57 μm (17.5%) at 6 wk and 2.53 μm (39.2%) at 20 wk (Fig. 4). In the *db/db* group we also found significantly thinner NFL+GCL at both 10 wk and 16 wk of age compared with age-matched controls, again replicating the findings in people with DM and also showing that the thinning is not a toxic effect of STZ administration. As in humans, the thinning caused by DM in STZ-treated mice is progressive and is significantly accelerated compared with thinning in the age-matched control group. Immunohistochemistry at 6 wk after DM induction showed no reduction in GC density in the STZ-treated group, but at 20 wk there was a significant loss of GC density (Fig. 4), confirming the OCT findings in humans and mice and the immunohistochemistry findings in donor eyes. These findings confirm the GC loss in STZ-treated mice as early as 10 wk and 16 wk described by others (25) and are in line with a study in diabetic rats and human donor eyes showing neural apoptosis as early as 4 wk after DM onset, although a comprehensive analysis comparing temporal changes in the vasculature and inner retinal thinning was not performed in that study (20).

The STZ mouse model allowed us to study the sequence of events. Specifically, we found (*i*) no difference between the density of endothelial-supporting retinal pericytes in the STZ-treated group compared with age-matched controls; (*ii*) no difference in the number of acellular capillaries in the STZ-treated group compared with age-matched controls; (*iii*) no difference in pericyte density in the NFL/GCL and inner and outer vascular

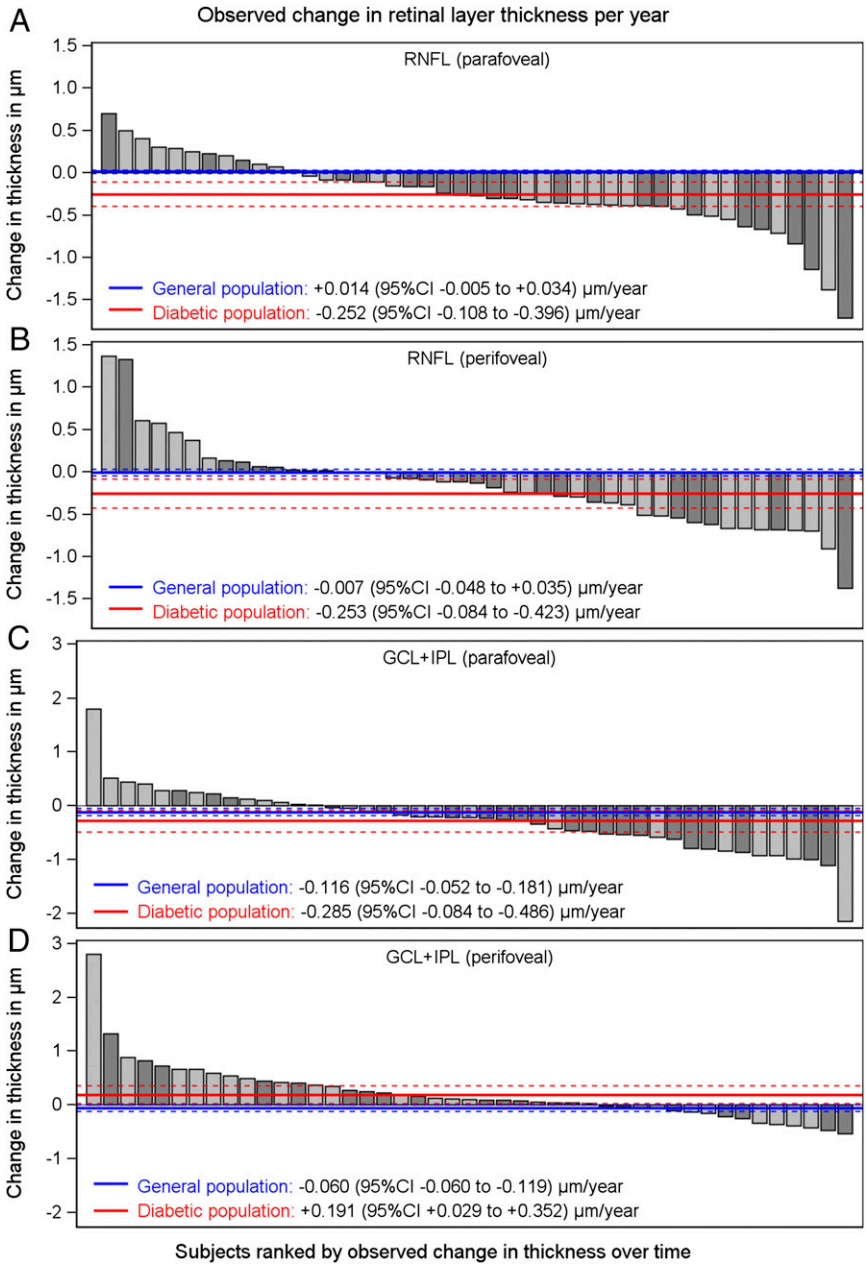

Fig. 2. Subjects with DM and no or minimal DR ($n = 45$) show significant neuroretinal thinning over time. (*A*–*C*) Observed changes in retinal layer thickness per year, with subjects ranked (from left to right) by observed change in layer thickness over time, showing significant thinning of the parafoveal NFL (*A*), perifoveal NFL (*B*), and perifoveal GCL+IPL (*C*). (*D*) Nonsignificant changes in parafoveal GCL+IPL. All layer thicknesses were measured by Stratus OCT imaging analysis over a 4-y study period and are demonstrated by the linear mixed regression models shown in Table 1. Each vertical bar represents the change in thickness per year in the parafoveal and perifoveal NFL and GCL+IPL regions for each subject. Dark-gray bars represent subjects without DR progression; light-gray bars represent subjects with DR progression. The solid and dotted red lines show the mean and 95% CI change in subjects in this study, respectively (model derived as in Table 1). Solid and dotted blue lines show the previously published mean and 95% CI loss, respectively, in normal control subjects (14).

plexus (Fig. 4); and (*iv*) no difference using the vessel stain IB4 at 20 wk; all confirming that there were no differences in the vasculature of the STZ-treated mice and controls. Although in human donor eyes we were able to determine that RDN occurs in the absence of DR or capillary loss, these results in mice show that RDN occurs before any evidence of microvascular damage as defined by Cogan (8).

RDN is clinically relevant, for example affecting the visual outcome after successful treatment of diabetic macular edema (26). Retinal neurodegeneration at the cellular and functional (ERG) level has been described previously (27) in another mouse model of spontaneous DM. The functional consequences of progressive RDN are not yet clear, although they have been gaining recognition (4, 5, 28). In a previous study, using the same OCT image analysis methods, we reported a high correlation (0.68) between perimetric functional loss and RDN in people with DM and no or minimal DR (4). In another recent study we found that the difference in average thickness between patients with early glaucoma (<6 dB perimetric loss) and those with severe glaucoma (>12 dB loss) is 5–8 µm for the NFL and 1–8 µm for the GCL (29). The present results show that, on average, DM causes a progressive loss of 0.25 µm/y in the NFL and a loss of

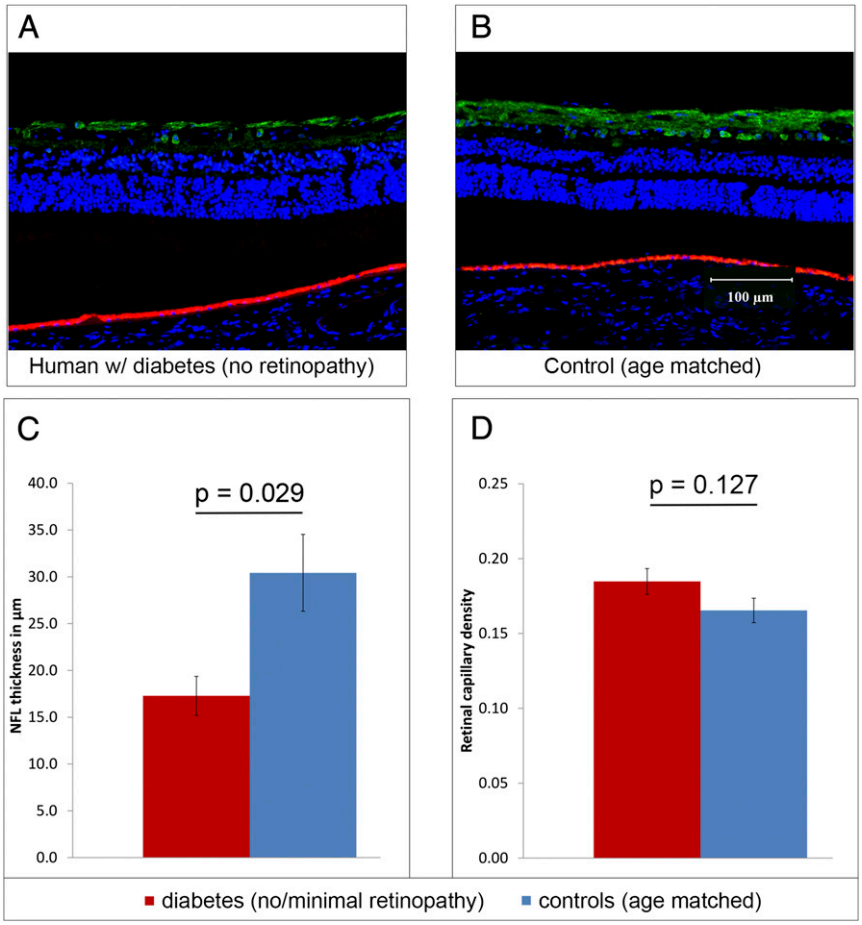

Fig. 3. (*A* and *B*) Sections of eyes from human donors with DM and no retinopathy (*A*) and from age-matched controls (*B*) stained with γ-synuclein antibody to immunolabel GCs and the NFL (green); DAPI nuclear counterstaining is blue; the red-orange signal at the level of the RPE is caused by autofluorescence. (*C*) The NFL was significantly thinner in the diabetic eyes ($n = 6$) than in controls ($n = 5$). (*D*) Retinal capillary density was measured from whole-mount sections; vessels were immunolabeled with biotinylated UEA-I followed by avidin conjugated to Texas Red (Fig. S4). No significant difference in retinal capillary density was found in eyes from diabetic donors ($n = 6$) and from controls ($n = 5$).

0.29 μm/y in the GCL; thus after 10–20 y, the loss caused by RDN is similar in magnitude to that in severe glaucoma, although it may be more diffuse than the typical scotomata in glaucoma. Although glaucoma patients require regular perimetric examinations, such functional studies are not typically used in routine care for people with DM. It will be critical to expand on these previous studies to determine the short- and long-term visual consequences of RDN.

Clinicians-in-training are not made aware of RDN as a pathologic process resulting from DM (30), although the entity is well recognized in diabetic animal and human studies (1, 3, 27, 31, 32). One reason is that any changes in the diabetic retina are almost always attributed to the frequently recognized microvascular alterations culminating in ischemia of the retina and subsequent up-regulation of cytokines such as vascular endothelial growth factor (8, 33–37). Our findings show that inner retinal changes do occur before the markers of microvasculopathy in the retina, as defined by Cogan in 1961 (8). Nevertheless, whether RDN plays a role in the development of retinal ischemia in DM is unclear. A second reason is that, before the advent of OCT and automated image analysis, which allows the detection of submicrometer changes, substantially below the resolution of the OCT device's individual A-scans, it was impossible to quantify any in vivo effect of RDN (38). Third, there currently are no treatment or management options to mitigate RDN. Although we found that RDN progression is independent of the HbA1C level, the key marker for hyperglycemia over the previous 3 mo, our results do not establish whether relatively poor glycemic control will result in more rapid neuroretinal degeneration. In addition, although current therapies for DR, such as the monthly intravitreal administration of anti-VEGF (39) and steroids, are highly successful clinically, there is some concern that the former may cause or accelerate retinal neurodegeneration in rodents (40). As the functional visual consequences of RDN are further elaborated, neuroprotective strategies developed for glaucoma and other neurodegenerative diseases may merit study for RDN, especially during anti-VEGF treatment (32, 41, 42).

The goal of this study was to determine the temporal relationship between RDN and microvascular manifestations of DM, including DR. We did not focus on identifying the pathophysiological mechanisms, because compelling mechanistic data from previous studies demonstrate neural apoptosis, glial cell reactivity, and numerous aberrant biochemical pathways associated with RDN that appear to be independent of vascular changes (3, 32, 43, 44). In the retina, glial, neural, and vascular cells are closely associated in a so-called "neurovascular unit" to maintain the homeostasis necessary for normal neuroretinal function (1). Intriguingly, although HbA1C is well known to affect microvasculopathy and DR in people with DM, we found no relationship between HbA1C and the progression of RDN (45), possibly indicating that their pathophysiologies are initially independent; this possibility is also suggested by results from the Epidemiology of Diabetes Interventions

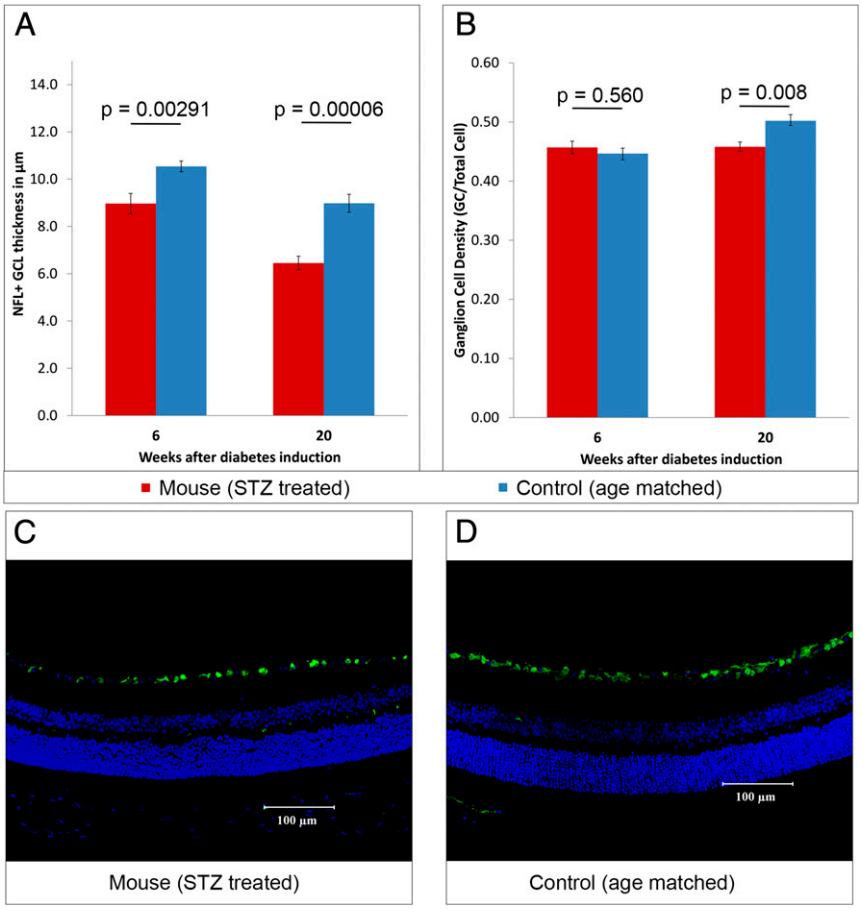

Fig. 4. (*A*) SD-OCT analysis (Fig. S5) showed significant NFL+GCL thinning in the mice with STZ-induced DM as compared with age-matched controls at both 6 wk ($n = 21$ diabetic mice, 15 controls) and 20 wk ($n = 11$ diabetic mice, 10 controls) of DM duration. (*B*) GC density is not significantly different in DM and control mice at 6 wk but is significantly lower in diabetic mice than in controls at 20 wk ($n = 10$ diabetic mice, 10 controls). (*C* and *D*) Representative sections of the inner retina of mice with STZ-induced DM at 20 wk (*C*) and age-matched controls (*D*). Anti–γ-synuclein antibody was used to immunolabel GCs (green); DAPI nuclear counterstaining is shown in blue.

and Complications/Diabetes Control and Complications Trial study showing that HbA1C explains only 9.1–14.1% of the variance in development of DR (45).

There are varying definitions of the first manifestation of microvascular damage in DR. The most widely accepted earliest preclinical sign is the loss of pericytes, using trypsin-digestion methods first described by Cogan et al. (8); this was the primary marker we used in the mouse experiments. On the other hand, microaneurysms are the first clinical sign of DR as established by Friedenwald et al. (9) [although others have proposed capillary nonperfusion (46)] and were the marker we used in the longitudinal study. We did not perform fluorescein angiography, however, because even small areas of capillary nonperfusion are typically accompanied by microaneurysms and/or hemorrhages noted on fundus photography at the same visit; nor did we perform OCT angiography, which has the potential to quantify capillary nonperfusion, because it has become available only recently. Moreover, immunohistochemistry results in eyes from donors with DM and no or minimal DR show that neurodegeneration occurs without evidence of capillary loss as compared with controls (Fig. 2) (34).

In summary, neuroretinal degeneration precedes microvasculopathy in people with DM, and these findings were confirmed in two different mouse models of DM using both OCT image analysis and immunohistochemistry. The retinal neurodegeneration is not mediated by retinal microvascular disease in the form of microscopic capillary loss or the earliest manifestation of DR, i.e., pericyte loss, but is primarily related to DM duration. These results suggest that RDN is not ischemic in origin and represent a shift in our understanding of the pathophysiology of this complication of DM that potentially affects vision in all people with DM.

Methods

Study Approval. The research adhered to the tenets of the Declaration of Helsinki. Institutional Review Board approval was obtained at both the University of Iowa and the Academic Medical Center at the University of Amsterdam, and all participants provided written informed consent before inclusion in study.

All animal studies were performed in accordance with the guidelines of the Association for Research in Vision and Ophthalmology and were approved by the Institutional Animal Care and Use Committee of the University of Iowa.

Donor eyes were obtained from the Iowa Lions Eye Bank within 9 h of death (Table S2), following informed consent of the donor's next of kin. Approval was obtained from the Internal Review Board of the University of Iowa, and all research adhered to the tenets of the Declaration of Helsinki.

Longitudinal Observational Study of Neuroretina in DM. Subjects with type 1 DM were recruited from the outpatient clinic of the Department of Internal Medicine at the Academic Medical Center at the University of Amsterdam, the Netherlands, between July 2004 and June 2005. Patients were included if they had no DR or minimal DR as determined by a retinal specialist through slit-lamp stereo biomicroscopy and fundus photographs (TRC-50IX; Topcon Corporation). No and minimal DR were defined by the International Clinical Diabetic Retinopathy Disease Severity Scale, on which minimal DR means microaneurysms only, or equal to or less than level 20 according to the Early Treatment Diabetic Retinopathy Study criteria (47). Patients with current or a

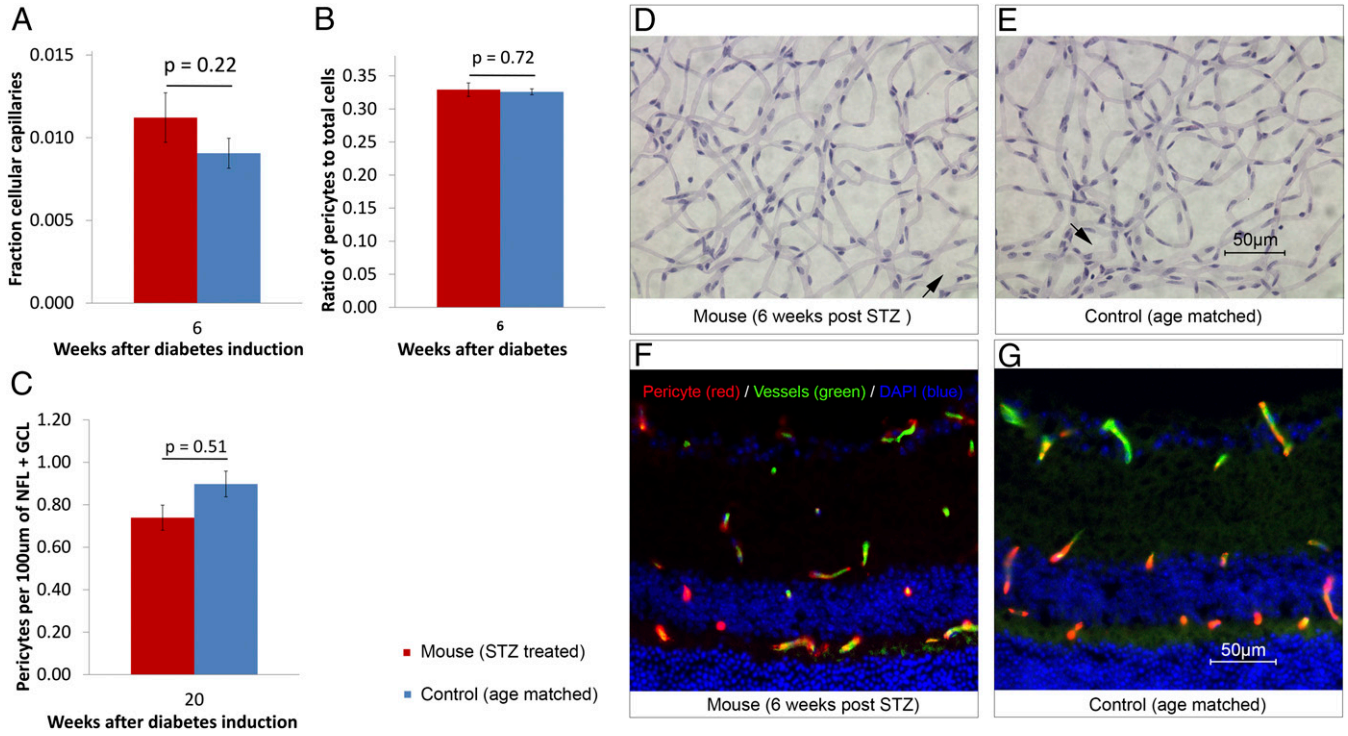

Fig. 5. (*A* and *B*) STZ-induced DM in a mouse model does not significantly affect acellular capillaries ($n = 6$ diabetic mice, 6 controls) (*A*) or pericyte density ($n = 6$ diabetic mice, 6 controls) (*B*) at 6-wk DM duration. (*C*) There was a trend favoring pericyte dropout in mice at 20 wk of DM duration, but this trend was not significant ($n = 8$ diabetic mice, 8 controls). (*D* and *E*) Images of trypsin-digested whole-mount retina show similar numbers of acellular capillaries (black arrows) in diabetic (*D*) and control (*E*) mice. (*F* and *G*) Histologic sections of retinas from diabetic (*F*) and control (*G*) mice dual-immunolabeled with NG-2 (red) and IB4 (green) show similar numbers of pericytes and vessels. DAPI nuclear counterstaining is shown in blue.

history of diabetic macular edema were excluded. Other exclusion criteria were refractive errors over S+5 or under S–8 diopters, BCVA below 0.1 (logMAR notation), significant media opacities, previous ocular surgery, and a previous diagnosis of glaucoma, uveitis, or other retinal disease. All patients underwent imaging at baseline and approximately every 12 mo thereafter, as well as ophthalmic and general examinations including blood pressure and HbA1c. Visual acuity was measured using an Early Treatment Diabetic Retinopathy Study chart at 4 m (48). Two cross-sectional studies of these subjects have been published previously, one using time-domain OCT (TD-OCT) and one using spectral domain OCT (SD-OCT), showing comparable thinning of the inner retina (4, 15, 16).

Visit Protocol, OCT, and Fundus Imaging. At each visit, subjects were imaged with Stratus OCT (Model 3000; Carl Zeiss Meditec; software version 4.0.1). The fast macular-thickness OCT scan protocol was used. This scan protocol obtains six cross-sectional B-scans, 6 mm in length, at equally spaced angular orientations (30°) in a radial pattern centered on the fovea. Retinal color images were taken with a Topcon NW6 Fundus camera and were evaluated by a retinal specialist according to a previously published standardized protocol (grade 0 = no microaneurysms; grade 1 = 0–5 microaneurysms; grade 2 = 5–10 microaneurysms; grade 3 = 10–20 microaneurysms; grade 4 = more than 20 microaneurysms) (4, 15, 16). DR progression was defined by patients with no DR progressing to minimal or more DR at the next visit or by the number of microaneurysms increasing by at least one grade from any previous visit. Although SD-OCT allows a higher number of A-scans and thus higher resolution than Stratus OCT, we used TD-OCT in this prospective longitudinal study because SD-OCT was not available at the start of the study. The use of TD-OCT throughout the study ensured that the images collected were directly comparable. In a prior study we used Topcon SD-OCT to confirm neuroretinal thinning of the subjects with DM as compared with normal controls using cross-sectional analysis at the 4-y visit (49). Other studies also have used TD-OCT (50, 51), and we and others have shown that outcome does not differ between TD- and SD-OCT (4, 16, 49). The thickness of the NFL and GCL+IPL in the macula was quantified for parafoveal and perifoveal rings centered on the fovea (see below).

OCT Automated Image Analysis. All OCT scans were analyzed automatically with the 3D segmentation algorithm referred to as the Iowa Reference Algorithms, and the six retinal layers that can be identified in the six cross-sectional B-scans using Stratus OCT automated segmentation were interpreted as follows (from the inner to the outer surface): NFL, GCL+IPL, inner nuclear layer (INL), outer plexiform layer (OPL), outer nuclear layer (ONL) + inner segments (of the photoreceptors), and outer segments (of the photoreceptors). These algorithms have been validated extensively (52). On Stratus OCT it is not possible to differentiate the boundary between the GCL and the IPL reliably, so these were combined, as we have always done (4, 16, 49). After segmentation, two retinal regions of interest were defined: the parafoveal region, a donut-shaped ring centered on the fovea with an inner diameter of 1 mm and an outer diameter of 3 mm, and the perifoveal region, with an inner diameter of 3 mm and outer diameter of 6 mm (Fig. S1). The Iowa Reference Algorithms are available to researchers for free in the public domain at www.iibi.uiowa.edu/content/shared-software-download/.

Human Donor Eye Studies. Whole eyes or superotemporal and macular wedges were fixed in toto in 4% paraformaldehyde in PBS. The average age of eyes used in this study was 77.8 y in the DM group and 72.5 y in the control group with an age range of 49–86 y (Table S2); controls were matched in age as closely as possible (noted as "similarly aged" in the text). Exclusion criteria for all subjects consisted of a diagnosis of glaucoma or suspected glaucoma, ocular hypertension, or a history of any condition affecting the retina including age-related macular degeneration, vein occlusion, uveitis, and vitreoretinal surgery. Donor eye records, fundus photographs, and gross eyecups were reviewed in detail to ensure that patients in the DM group did not have more than a single isolated hemorrhage, consistent with the condition of no or minimal nonproliferative diabetic retinopathy (NPDR); eyes with a history of macular edema, moderate, severe or proliferative DR, laser treatment, or intraocular injections were excluded (Table S2).

Tissue Preparation and Immunolabeling. Four-millimeter biopsy punches centered 6 mm superior to the fovea were cryoprotected in serial sucrose solution and embedded for cryostat sectioning, as described previously (53). Cryostat sections (10 μm) were collected and stained with 1 μg/mL anti–γ-synuclein (Abcam) to immunolabel GCs, and DAPI was used to counterstain nucleated cells. Additional 4-mm biopsy punches centered 6 mm inferior to the fovea were collected for flat-mount histochemistry with biotinylated-conjugated

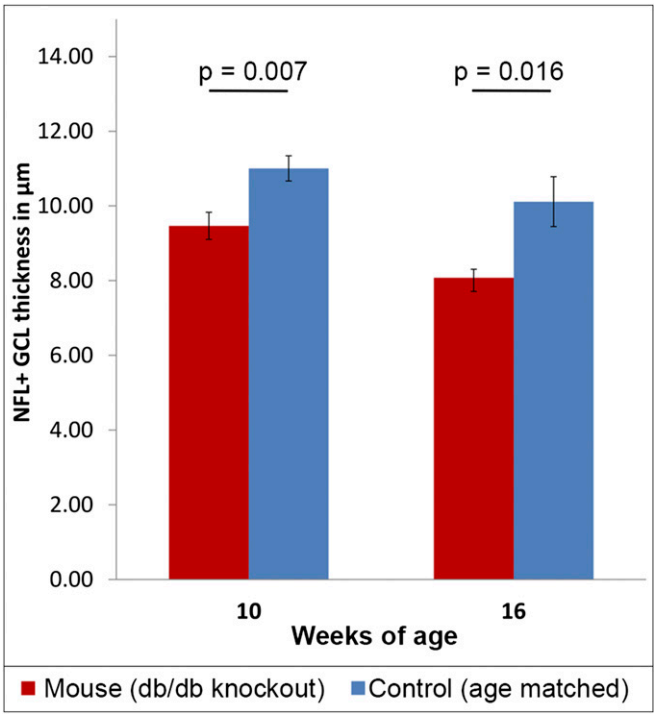

Fig. 6. Progressive thinning of the NFL/GCL layer also is seen on OCT imaging analysis in 10-wk-old (n = 18 diabetic mice, 14 controls) and 16-wk-old (n = 18 diabetic mice, 9 controls) *db/db* mice, which have a spontaneous young-onset form of DM.

Ulex europaeus agglutinin-I (UEA-I) (Vector Laboratories) followed by incubation with avidin conjugated to Texas Red to visualize retinal vasculatures (54). Negative controls for immunostaining were performed in parallel by omission of primary antibodies. Sections were imaged with an Olympus BX41 fluorescence microscope and analyzed in ImageJ (55).

Determination of Donor Eye GC Density and NFL Thickness. All morphometric measurements were combined from two masked graders. Analysis of each grader's dataset separately showed statistically significant differences between the diabetic and control groups. To determine GC density and NFL thickness, the number of cells positively labeled with anti–γ-synuclein and the length and thickness of retinal NFL were computed at 200-μm intervals in each 4-mm punch. A total of 30–40 images obtained with a high-power (20×) objective from 8–12 sections of each donor eye were analyzed.

Determination of Donor Eye Retinal Capillary Density. Following visualization of UEA-I, images were analyzed in ImageJ (55). Local threshold was optimized automatically for maximal capillary contrast using Phansalkar's approach (56) with a round window, with (dimensionless) algorithmic standard parameters k = 0.01–0.05 depending on the amount of background fluorescence, r = 0.5, P = 2, and q = 10. After thresholding, a single morphological closing and then erosion was performed to remove single pixels erroneously thresholded as capillary. All regions of interest containing capillaries outside arterioles and venules and larger vessels were selected, and capillary density was quantified as the fraction of pixels that were part of a capillary in the regions of interest. In other words, a capillary density 0.2 means that 20% of the (projected) fluorescence image is covered by capillaries (Fig. S3). Capillary density was averaged over all 21 or 22 images representing the 4-mm punches for each eye.

Animal Studies. For the STZ-induced mouse model of type 1 DM, C57BL/6J male mice (The Jackson Laboratory) at 8–12 wk of age were randomly assigned to diabetic (STZ-induced) or nondiabetic control groups. In the STZ group, DM was induced between 8 wk and 10 wk of age by i.p. injections of STZ (Sigma Chemical Co.); mice were injected with 60 mg/kg STZ daily for 5 d. Serum glucose levels were measured 3 d after the last injection and were monitored monthly thereafter. If serum glucose was less than 300 mg/dL, mice were injected for an additional 3 d with 50–60 mg/kg of STZ (Fig. S4). Only mice with glucose levels consistently elevated above 350 mg/dL were considered diabetic and included in the study (Fig. S4). Severely diabetic mice were treated s.c. with 2.7 U/20 g insulin (Sigma Chemical Co.) daily. Serum glucose levels in the age-matched C57BL/6J male control mice averaged 120–220 mg/dL. Randomly assigned STZ-treated mice underwent OCT imaging 6 wk (approximate age 16 wk) and 20 wk (approximate age 30 wk) after DM was confirmed and were killed at these time points.

Genetically modified B6.BKS(D)-*Lepr^{db}* /J mice (*db/db*; The Jackson Laboratory) were used as a model of type 2 DM not requiring exogenous STZ, with spontaneous, young-onset DM that persists until 16 wk of age. Blood glucose of these *db/db* mice was monitored weekly, and mice with a glucose level >350 mg/dL were considered diabetic. Online STZ was administered starting at 16 wk to maintain hyperglycemia once euglycemia began. The *db/db* mice underwent OCT imaging at age 10 wk and 16 wk.

For the control group, we used the age-matched C57BL/6J mice that were not randomized to receive STZ. These mice were OCT imaged at age 8–10 wk (controls for the *db/db* group were imaged at age 10 wk, and controls for the STZ group were imaged at baseline), at age 16 wk (controls for the *db/db* group were imaged at age 16 wk, and controls for the STZ group were imaged 6 wk after DM induction), and at age 30 wk (controls for the STZ group were imaged at 20 wk after DM induction). These mice were killed at either 16 wk or 30 wk of age.

Mouse OCT Imaging and Analysis. After the animals were anesthetized with ketamine/xylazine (87.5 mg/kg ketamine, 12.5 mg/kg xylazine), the pupils were dilated with 1% tropicamide (Akorn, Inc.). To lubricate the eyes, 0.2% hypromellose eye gel (GenTeal; Novartis) was used. The animals were placed onto an adjustable cassette for SD-OCT imaging (Bioptigen Envisu R2200), and the cassette was connected to a platform that allowed 3D alignment.

OCT scanning was initially directed to the center (posterior pole) of the mouse eye, facilitated by the aiming laser beam of the scanner. For the volume scans, the aiming laser was centered on the optic nerve head (Fig. S5). The dimension of the scan (in depth and transverse extent) was adjusted until optimal signal intensity and contrast were achieved. OCT volume dimensions were 400 × 400 × 1,024 voxels (1.4 × 1.4 × 1.566 mm^3). After storage, offline automated segmentation of the boundaries of the inner limiting membrane (ILM), GCL, IPL, INL, OPL, OPL, external limiting membrane, inner/outer photoreceptor segment (IS/OS) junction, retinal pigment epithelium (RPE) superior surface, and Bruch's membrane was performed using the Iowa Reference Algorithms for 3D automated layer segmentation; the thickness of the NFL+GCL was quantified as the distance between the ILM and the bottom surface of the GCL (52, 57). Current SD-OCT technology does not allow the NFL to be differentiated from the GCL in mice. The Iowa Reference Algorithms are available for free in the public domain at www.iibi.uiowa.edu/content/shared-software-download/ (52), and a recent independent validation showed superior performance for the inner retina in mice (58).

Preparation and Immunolabeling of Mouse Tissue. Mice were lethally injected with ketamine/xylazine (175.0 mg/kg ketamine and 25.0 mg/kg xylazine); after cervical dislocation, eyes were enucleated and fixed with PBS containing 4% paraformaldehyde at room temperature for 4 h. The cornea and lens were removed carefully; then the mouse eyes were cryoprotected by sequential immersion in 5%, 10%, and 20% (wt/vol) sucrose solutions and were embedded in Tissue-Tek Optimum Cutting Temperature (OCT) compound (Sakura) in liquid nitrogen. Transverse 10-μm serial frozen sections were cut and mounted onto Superfrost Plus glass slides (Thermo Scientific) and stored at −80 °C until use. One eye per mouse from each experimental group was used. Every 20th frozen section throughout the entire eye was selected for immunohistochemical quantitative assessment. Sections were treated and blocked for 30 min at room temperature with 0.3% Triton/0.1% BSA/PBS, incubated overnight (4 °C) with 0.5 μg/mL anti–γ-synuclein (Abnova), 2 μg/mL anti-NG2 (Abcam), or 2.5 μg/mL biotinylated lectin GSL-IB4 (Vector Laboratories) to immunolabel GCs, pericytes, or blood vessels, respectively. After washing with PBS, sections were probed with 7.5 μg/mL Cy2 anti-mouse, Cy3 anti-mouse (Jackson ImmunoResearch Laboratories), or 5 μg/mL Dylight 488 streptavidin (Vector Laboratories) secondary fluorescence antibody for 1 h at room temperature and then were mounted with anti-fade medium with DAPI. Negative controls for immunohistochemistry were performed in parallel by using isotype-matched IgG. Images were captured by an Olympus BX41 fluorescence microscope, and were digitally analyzed using Image J software (55).

Mouse Morphometry Analysis. All morphometric measurements were made by two masked graders. Analysis of each grader's dataset showed statistically significant differences between the same groups. Assessment of acellular

capillaries was performed on trypsin-digested retina as described previously (59). To determine GC density (GC/total cells), the number of anti–γ-synuclein–immunolabeled cells and the total number of nucleated cells in the superficial layer were measured in every 20th section (i.e., every 200 μm). A total of 40–50 images taken with a high-power (20×) objective from 8–12 sections of each eye per animal were quantified. The number of pericytes per area of vascular plexus was traced and computed by total number of anti-NG2–stained cells over the vascular plexus area in every 20th section (number of pericytes/1,000 μm^2 of the total vascular plexus area).

Statistical Analysis.

Longitudinal data. Statistical analysis was performed using SPSS software version 20.0 (SPSS Inc.) and SAS software version 9.2 (SAS Institute Inc.). ANOVA was used to assess differences in mean HbA1c, mean blood pressure, and mean BCVA in the four follow-up visits. In a previous study it was demonstrated that there was no statistical difference in the measurements in a subject's two eyes, and one eye was at random chosen for the present analysis (60). Changes over time in the thickness of the inner retinal layers were assessed using linear mixed regression models with a first-order autoregressive covariance structure to take into account that repeated measurements on the same subject over time are highly correlated and that observations on the same subject that are closer in time are more highly correlated than measurements at times further apart. The correlation between two measurements within the same subject decreases exponentially as the length of time between the measurements increases. The mixed-effects model is also robust to missing data and can handle uneven intervals between the repeat measurements. The model was adjusted for age, sex, DM duration, HbA1c, DR at inclusion, and progression of DR, which were included as fixed effects in the model. Age, HbA1c, and progression of DR were included in the model as time-updated covariates. Four models were used, for parafoveal and perifoveal NFL and parafoveal and perifoveal GCL+IPL, respectively. The primary research objective was to test if there was progressive thinning of the parafoveal and perifoveal NFL and/or GCL+IPL. We considered 95% CIs that did not straddle zero to be statistically significant. All reported *P* values are two-sided.

Human donor eye data. Morphometric data were averaged on a per-eye basis. Data were analyzed by two-tailed Student *t* test to compare two groups of variables. One-way ANOVA followed by Bonferroni post hoc analysis was used to compare the differences in multiple groups using SPSS software 11.0 (SPSS Inc.). Results are expressed as mean ± 95% CI. $P < 0$ 0.05 was considered statistically significant. The intraclass correlation coefficient (ICC) was used in each study to measure the reliability of the rating between two graders with a 95% CI. The reliability of each measurement from two graders was 0.86 for human donor eye NFL thickness, 0.94 for mouse GC density, 0.97 for mouse acellular capillary assessment, and 0.90 for mouse pericyte density. There was no significant difference between the two observers in all assessments.

Mouse data. Morphometric data were averaged on a per-eye basis. Data were analyzed by two-tailed Student *t* test to compare two groups of variables. One-way ANOVA followed by Bonferroni post hoc analysis was used to compare the differences in multiple groups using SPSS software 11.0 (SPSS Inc.). Results are reported as mean ± 95% CI and as mean ± SEM in graphs. $P < 0$ 0.05 was considered statistically significant. The ICC was used in each study to measure the reliability of the rating between two graders with a 95% CI. The reliability of each measurement from two graders was 0.86 for human donor eye NFL thickness, 0.94 for mouse GC density, 0.97 for mouse acellular capillary assessment, and 0.90 for mouse pericyte density. There was no significant difference between the two observers in all assessments.

ACKNOWLEDGMENTS. Funding for this work was provided by National Institutes of Health Grants R01EY018853, R01EY019112, R01EB004640, R01EY016379, and R01EY017066; Research to Prevent Blindness; Wynn Institute for Vision Research; Arnold and Mabel Beckman Initiative for Macular Research; and The Netherlands Organization for Research (ZonMW). This work was supported in part by Merit Review Award I01 CX000119 from the US Department of Veterans Affairs Rehab Service; contents do not represent the views of the US Department of Veterans Affairs or the United States Government.

1. Antonetti DA, Klein R, Gardner TW (2012) Diabetic retinopathy. *N Engl J Med* 366(13): 1227–1239.
2. Antonetti DA, et al.; JDRF Diabetic Retinopathy Center Group (2006) Diabetic retinopathy: Seeing beyond glucose-induced microvascular disease. *Diabetes* 55(9): 2401–2411.
3. Stem MS, Gardner TW (2013) Neurodegeneration in the pathogenesis of diabetic retinopathy: Molecular mechanisms and therapeutic implications. *Curr Med Chem* 20(26):3241–3250.
4. van Dijk HW, et al. (2011) Association of visual function and ganglion cell layer thickness in patients with diabetes mellitus type 1 and no or minimal diabetic retinopathy. *Vision Res* 51(2):224–228.
5. Realini T, Lai MQ, Barber L (2004) Impact of diabetes on glaucoma screening using frequency-doubling perimetry. *Ophthalmology* 111(11):2133–2136.
6. van Elderen SG, et al. (2010) Progression of brain atrophy and cognitive decline in diabetes mellitus: A 3-year follow-up. *Neurology* 75(11):997–1002.
7. Adams AJ, Bearse MA, Jr (2012) Retinal neuropathy precedes vasculopathy in diabetes: A function-based opportunity for early treatment intervention? *Clin Exp Optom* 95(3):256–265.
8. Cogan DG, Toussaint D, Kuwabara T (1961) Retinal vascular patterns. IV. Diabetic retinopathy. *Arch Ophthalmol* 66:366–378.
9. Friedenwald JS (1950) Diabetic retinopathy. *Am J Ophthalmol* 33(8):1187–1199.
10. Papachristodoulou D, Heath H, Kang SS (1976) The development of retinopathy in sucrose-fed and streptozotocin-diabetic rats. *Diabetologia* 12(4):367–374.
11. Mizutani M, Kern TS, Lorenzi M (1996) Accelerated death of retinal microvascular cells in human and experimental diabetic retinopathy. *J Clin Invest* 97(12):2883–2890.
12. Midena E, et al. (1989) Studies on the retina of the diabetic db/db mouse. I. Endothelial cell-pericyte ratio. *Ophthalmic Res* 21(2):106–111.
13. Kern TS, Engerman RL (1996) A mouse model of diabetic retinopathy. *Arch Ophthalmol* 114(8):986–990.
14. Demirkaya N, et al. (2013) Effect of age on individual retinal layer thickness in normal eyes as measured with spectral-domain optical coherence tomography. *Invest Ophthalmol Vis Sci* 54(7):4934–4940.
15. van Dijk HW, et al. (2009) Selective loss of inner retinal layer thickness in type 1 diabetic patients with minimal diabetic retinopathy. *Invest Ophthalmol Vis Sci* 50(7): 3404–3409.
16. van Dijk HW, et al. (2012) Early neurodegeneration in the retina of type 2 diabetic patients. *Invest Ophthalmol Vis Sci* 53(6):2715–2719.
17. Eisma JH, Dulle JE, Fort PE (2015) Current knowledge on diabetic retinopathy from human donor tissues. *World J Diabetes* 6(2):312–320.
18. Verma A, et al. (2012) Does neuronal damage precede vascular damage in subjects with type 2 diabetes mellitus and having no clinical diabetic retinopathy? *Ophthalmic Res* 47(4):202–207.
19. Feit-Leichman RA, et al. (2005) Vascular damage in a mouse model of diabetic retinopathy: Relation to neuronal and glial changes. *Invest Ophthalmol Vis Sci* 46(11): 4281–4287.
20. Barber AJ, et al. (1998) Neural apoptosis in the retina during experimental and human diabetes. Early onset and effect of insulin. *J Clin Invest* 102(4):783–791.
21. Beck RW, et al.; Diabetic Retinopathy Clinical Research Network (DRCR.net) (2009) Three-year follow-up of a randomized trial comparing focal/grid photocoagulation and intravitreal triamcinolone for diabetic macular edema. *Arch Ophthalmol* 127(3): 245–251.
22. Ooto S, et al. (2011) Effects of age, sex, and axial length on the three-dimensional profile of normal macular layer structures. *Invest Ophthalmol Vis Sci* 52(12):8769–8779.
23. Phipps JA, Fletcher EL, Vingrys AJ (2004) Paired-flash identification of rod and cone dysfunction in the diabetic rat. *Invest Ophthalmol Vis Sci* 45(12):4592–4600.
24. Sim DA, et al. (2014) Quantitative analysis of diabetic macular ischemia using optical coherence tomography. *Invest Ophthalmol Vis Sci* 55(1):417–423.
25. Martin PM, Roon P, Van Ells TK, Ganapathy V, Smith SB (2004) Death of retinal neurons in streptozotocin-induced diabetic mice. *Invest Ophthalmol Vis Sci* 45(9): 3330–3336.
26. Bonnin S, Tadayoni R, Erginay A, Massin P, Dupas B (2015) Correlation between ganglion cell layer thinning and poor visual function after resolution of diabetic macular edema. *Invest Ophthalmol Vis Sci* 56(2):978–982.
27. Bogdanov P, et al. (2014) The db/db mouse: A useful model for the study of diabetic retinal neurodegeneration. *PLoS One* 9(5):e97302.
28. Parisi V, Uccioli L (2001) Visual electrophysiological responses in persons with type 1 diabetes. *Diabetes Metab Res Rev* 17(1):12–18.
29. Bogunović H, et al. (2014) Relationships of retinal structure and humphrey 24-2 visual field thresholds in patients with glaucoma. *Invest Ophthalmol Vis Sci* 56(1):259–271.
30. American Academy of Ophthalmology (2015–2016) *Retina and Vitreous Basic and Clinical Science Courses Series* (BCSC) (American Academy of Ophthalmology, San Francisco), Vol 12.
31. Hombrebueno JR, Chen M, Penalva RG, Xu H (2014) Loss of synaptic connectivity, particularly in second order neurons is a key feature of diabetic retinal neuropathy in the Ins2Akita mouse. *PLoS One* 9(5):e97970.
32. Simo R, Hernandez C, and the European Consortium for the Early Treatment of Diabetic Retinopathy (2014) Neurodegeneration in the diabetic eye: New insights and therapeutic perspectives. *Trends Endocrinol Metab* 25(1):23–33.
33. Lorenzi M, Gerhardinger C (2001) Early cellular and molecular changes induced by diabetes in the retina. *Diabetologia* 44(7):791–804.
34. Bek T (1994) Transretinal histopathological changes in capillary-free areas of diabetic retinopathy. *Acta Ophthalmol (Copenh)* 72(4):409–415.
35. Bloodworth JM, Jr (1962) Diabetic retinopathy. *Diabetes* 11:1–22.
36. Wolter JR (1961) Diabetic capillary microaneurysms of the retina. *Arch Ophthalmol* 65:847–854.
37. Aiello LP, et al. (1994) Vascular endothelial growth factor in ocular fluid of patients with diabetic retinopathy and other retinal disorders. *N Engl J Med* 331(22):1480–1487.
38. Abràmoff MD, et al. (2013) Human photoreceptor outer segments shorten during light adaptation. *Invest Ophthalmol Vis Sci* 54(5):3721–3728.

39. Martin DF, Maguire MG (2015) Treatment choice for diabetic macular edema. *N Engl J Med* 372(13):1260–1261.
40. Park HY, Kim JH, Park CK (2014) Neuronal cell death in the inner retina and the influence of vascular endothelial growth factor inhibition in a diabetic rat model. *Am J Pathol* 184(6):1752–1762.
41. Imai H, Singh RS, Fort PE, Gardner TW (2009) Neuroprotection for diabetic retinopathy. *Dev Ophthalmol* 44:56–68.
42. Kuehn MH, Fingert JH, Kwon YH (2005) Retinal ganglion cell death in glaucoma: Mechanisms and neuroprotective strategies. *Ophthalmol Clin North Am* 18(3):383–395, vi.
43. Obrosova IG, et al. (2006) Early diabetes-induced biochemical changes in the retina: Comparison of rat and mouse models. *Diabetologia* 49(10):2525–2533.
44. Fletcher EL, Phipps JA, Ward MM, Puthussery T, Wilkinson-Berka JL (2007) Neuronal and glial cell abnormality as predictors of progression of diabetic retinopathy. *Curr Pharm Des* 13(26):2699–2712.
45. Anonymous (1995) The relationship of glycemic exposure (HbA1c) to the risk of development and progression of retinopathy in the diabetes control and complications trial. *Diabetes* 44(8):968–983.
46. Klemen UM, Freyler H (1980) Courses of diabetic retinopathy. *Albrecht Von Graefes Arch Klin Exp Ophthalmol* 213(2):135–142.
47. Wilkinson CP, et al.; Global Diabetic Retinopathy Project Group (2003) Proposed international clinical diabetic retinopathy and diabetic macular edema disease severity scales. *Ophthalmology* 110(9):1677–1682.
48. Early Treatment Diabetic Retinopathy Study Research Group (1987) Treatment techniques and clinical guidelines for photocoagulation of diabetic macular edema. Early Treatment Diabetic Retinopathy Study Report Number 2. *Ophthalmology* 94(7):761–774.
49. Van Dijk HW, et al. (2009) Selective loss of inner retinal layer thickness in type 1 diabetic patients with minimal diabetic retinopathy. *ARVO Meeting Abstracts* 50(5): 3244.
50. Bressler SB, et al.; Diabetic Retinopathy Clinical Research Network Writing Committee (2014) Reproducibility of spectral-domain optical coherence tomography retinal thickness measurements and conversion to equivalent time-domain metrics in diabetic macular edema. *JAMA Ophthalmol* 132(9):1113–1122.
51. Martin DF, et al.; Comparison of Age-related Macular Degeneration Treatments Trials (CATT) Research Group (2012) Ranibizumab and bevacizumab for treatment of neovascular age-related macular degeneration: Two-year results. *Ophthalmology* 119(7):1388–1398.
52. Abramoff MD, Garvin M, Sonka M (2010) Retinal imaging and image analysis. *IEEE Rev Biomed Engin* 3:169–208.
53. Barthel LK, Raymond PA (1990) Improved method for obtaining 3-microns cryosections for immunocytochemistry. *J Histochem Cytochem* 38(9):1383–1388.
54. Mullins RF, Grassi MA, Skeie JM (2005) Glycoconjugates of choroidal neovascular membranes in age-related macular degeneration. *Mol Vis* 11:509–517.
55. Abramoff MD, Magalhaes PJ, Ram S (2004) Image Processing with ImageJ. *Biophotonics International* 11(7):36–42.
56. Phansalkar N, More S, Sabale A, Joshi M (2011) Adaptive local thresholding for detection of nuclei in diversity stained cytology images. *2011 International Conference on Communications and Signal Processing (ICCSP),* pp 218–220.
57. Antony BJ, et al. (2014) Automated 3D segmentation of intraretinal surfaces in SD-OCT volumes in normal and diabetic mice. *Transl Vis Sci Technol* 3(5):8.
58. Dysli C, Enzmann V, Sznitman R, Zinkernagel MS (2015) Quantitative analysis of mouse retinal layers using automated segmentation of spectral domain optical coherence tomography images. *Transl Vis Sci Technol* 4(4):9.
59. Yang Y, et al. (2012) Decrease in retinal neuronal cells in streptozotocin-induced diabetic mice. *Mol Vis* 18:1411–1420.
60. Biallosterski C, et al. (2007) Decreased optical coherence tomography-measured pericentral retinal thickness in patients with diabetes mellitus type 1 with minimal diabetic retinopathy. *Br J Ophthalmol* 91(9):1135–1138.